CELL WALL ORGANIC MATRIX COMPOSITION AND BIOMINERALIZATION ACROSS REEF-BUILDING CORALLINE ALGAE UNDER GLOBAL CHANGE[1]

Ellie Bergstrom [iD] [2]

School of Environment & Science and Australian Rivers Institute – Nathan Campus, Griffith University, 170 Kessels Road, Brisbane, Nathan, Queensland, 4111, Australia

Jelle Lahnstein, Helen Collins [iD]

Adelaide Glycomics, School of Agriculture, Food, and Wine, University of Adelaide, Waite Campus, Urrbrae, South Australia, 5064, Australia

Tessa M. Page [iD]

School of Environment & Science and Australian Rivers Institute – Nathan Campus, Griffith University, 170 Kessels Road, Brisbane, Nathan, Queensland, 4111, Australia

Vincent Bulone [iD]

Adelaide Glycomics, School of Agriculture, Food, and Wine, University of Adelaide, Waite Campus, Urrbrae, South Australia, 5064, Australia

College of Medicine & Public Health, Health Sciences Building, Flinders University, Bedford Park Campus, Sturt Road, Adelaide, South Australia, 5042, Australia

and Guillermo Diaz-Pulido [iD] [2]

School of Environment & Science, Coastal & Marine Research Centre and Australian Rivers Institute – Nathan Campus, Griffith University, 170 Kessels Road, Brisbane, Nathan, Queensland, 4111, Australia

Crustose coralline algae (CCA) are one of the most important benthic substrate consolidators on coral reefs through their ability to deposit calcium carbonate on an organic matrix in their cell walls. Discrete polysaccharides have been recognized for their role in biomineralization, yet little is known about the carbohydrate composition of organic matrices across CCA taxa and whether they have the capacity to modulate their organic matrix constituents amidst environmental change, particularly the threats of ocean acidification (OA) and warming. We simulated elevated pCO$_2$ and temperature (IPCC RCP 8.5) and subjected four mid-shelf Great Barrier Reef species of CCA to 2 months of experimentation. To assess the variability in surficial monosaccharide composition and biomineralization across species and treatments, we determined the monosaccharide composition of the polysaccharides present in the cell walls of surficial algal tissue and quantified calcification. Our results revealed dissimilarity among species' monosaccharide constituents, which suggests that organic matrices are composed of different polysaccharides across CCA taxa. We also observed that species differentially modulate composition in response to ocean acidification and warming. Our findings suggest that both variability in composition and ability to modulate monosaccharide abundance may play a crucial role in surficial biomineralization dynamics under the stress of OA and global warming.

Key index words: biomineralization; calcification; coral reefs; crustose coralline algae; global warming; monosaccharides; ocean acidification; organic matrix

Abbreviations: CCA, crustose coralline algae; DOC, dissolved organic carbon; GBR, Great Barrier Reef; IPCC, Intergovernmental Panel on Climate Change; OA, ocean acidification; pCO$_2$, partial pressure of CO$_2$; RCP, representative concentration pathway; SST, sea surface temperature; UNI, unidentified monosaccharide peak

INTRODUCTION

Crustose coralline algae (CCA) are benthic calcifying marine red macroalgae that play an integral role in the structural stability of the world's reefs.

However, due to ongoing anthropogenic ocean acidification (OA) and warming, it is established that calcifying organisms like CCA are some of the most negatively impacted, particularly on tropical coral reefs (Hofmann and Bischof 2014, Cornwall et al. 2019). The production of calcium carbonate ($CaCO_3$) in the form of high-magnesium (high-Mg) calcite crystals in their cell walls via calcification, and the accumulation of calcified cell layers allow CCA to contribute to reef accretion and consolidation of loose substrate (Steneck 1986, Adey 1998). Yet, these same high-Mg calcite skeletons are sensitive to the decreasing pH that characterizes OA, which can result in reduced calcification rates, increased dissolution, and even partial mortality, thus challenging reef integrity (Martin and Gattuso 2009, Diaz-Pulido et al. 2012, Nash et al. 2015). CCA also facilitate ecological functioning through the provision of substrate for invertebrate larval settlement across phyla, e.g., corals (Harrington et al. 2004), abalone (Daume et al. 1999), sea urchins (Rowley 1989), and polychaetes (Gee and Knight-Jones 1962). However, the magnitude of impact that OA and warming have on CCA skeletons varies across taxa (Hofmann and Bischof 2014), suggesting some might possess coping mechanisms that would allow them to uphold these ecological roles into the Anthropocene. Due to the limited availability of mechanistic information about calcification in CCA (Borowitzka and Larkum 1987, Cornwall et al. 2017, DeCarlo et al. 2019, McNicholl et al. 2019, Nash et al. 2019), the potential for $CaCO_3$ skeleton regulation remains unclear. To better understand the calcification dynamics in CCA under environmental change, greater knowledge of the mechanisms by which calcification occurs at the cellular and structural level is needed.

Calcium carbonate precipitation in CCA occurs in the cell wall, as opposed to corals or green calcifying algae (i.e., *Halimeda*) in which it occurs in the intercellular space (Goreau 1961, Borowitzka and Larkum 1987). Crystal nucleation can also occur intracellularly in other organisms such as coccolithophores (Brownlee and Taylor 2004). Calcification in CCA is associated with a cell wall organic matrix. Cell walls are largely made up of carbohydrate polymers that are organized into a latticework, or organic matrix, which provides the scaffolding necessary for mineralization to occur (Borowitzka and Larkum 1987, Bilan and Usov 2001, Nash et al. 2019). A bio-induced calcification mechanism in CCA proposes that $CaCO_3$ crystal nucleation on structural polysaccharides is induced when surrounded by a matrix fluid comprised of endogenous polysaccharides, i.e. inducing polysaccharides, and seawater (containing inorganic carbon and calcium/magnesium; Nash et al. 2019). These structural and inducing polysaccharides from the CCA matrix have been isolated and identified to an extent, where some are unique to corallines (i.e.,

corallinins; e.g., particular sulfated xylogalactans, or SXGs; Usov 1992, Usov et al. 1995, Takano et al. 1996, Usov and Zelinsky 2013), some are common across red algae (e.g., carageenans and agarans; Lee 2018), and others are present in multiple algal phyla (e.g., cellulose, alginates and chitin; Siegel and Siegel 1973, Rahman and Halfar 2014). The biomineralization-inducing function of particular carbohydrate polymers has been confirmed by studies that have isolated polysaccharides, specifically particular sulphated xylogalactans (SXGs), from coralline cell walls, and observed in vitro crystallization in the presence of calcium-containing seawater (Pavez et al. 2005). While it is presumed that the inducing polysaccharides would be positively correlated with crystal formation, the relationship between both inducing and structural polysaccharides and calcification is still poorly understood. It is also not presently understood whether a polysaccharide can possess both inducing and structural properties, and if this dual functionality could be context-dependent. Additionally, other matrix constituents suggested to be inhibitory (Borowitzka and Larkum 1987) are expected to be negatively correlated with $CaCO_3$ deposition, but these are also poorly characterized. Thus, it is still not clear how matrix constituents as a whole are related to the calcification process, whether matrix composition can be regulated by CCA, and perhaps more importantly, it is completely unknown whether increased seawater pCO_2 (reduced pH) and warming influence the composition of the organic matrix and consequently CCA calcification.

Recent data suggest that calcification is a biologically-induced process, rather than biologically controlled (Nash et al. 2019), but the degree of regulation that CCA possess over calcification is currently under debate. Research supports the ability of CCA to regulate the matrix fluid carbonate chemistry potentially as a means for controlling calcification (Cornwall et al. 2017, Comeau et al. 2018). Yet on the other hand, one of the characteristic features of bio-induced mineralization is that there is an absence of control over the calcifying fluid. Nash et al. (2019) argue that although the organism-produced fluid can be metabolically controlled, the porosity of the CCA surface allows free exchange of seawater, resulting in the final mixed matrix fluid being uncontrolled. Although, there is some evidence that CCA control the calcifying fluid chemistry (Cornwall et al. 2017, Comeau et al. 2018), the precipitation of high Mg-calcite crystals would also be largely dependent on the existence of a suitable cell-wall organic matrix (Borowitzka and Larkum 1987, Nash et al. 2019). To date, there is no information regarding the modulation of cell wall organic constituents in CCA under environmental change. As seawater temperature increases and pH decreases, it will be crucial to determine the effects these environmental factors have on organic matrix

composition and whether calcification is differentially affected across CCA taxa.

This study aimed to determine how monosaccharide composition of polysaccharides varies across species and whether CCA are capable of altering monosaccharide composition in carbohydrate polymers under environmental changes, in hopes of achieving a greater understanding of the relationship between the cell wall organic matrix and biomineralization. Ideally, the fine structure of polysaccharides must be determined to assess and confirm the importance of their function. However, due to the difficulty of obtaining enough biomass from CCA to finely characterize polysaccharides, their monosaccharide composition was determined in the first instance. Here we hypothesized that: (i) the monosaccharide composition of polysaccharides varies across CCA taxa, and (ii) CCA differentially shift the relative abundance of monosaccharide constituents in their cell walls, as well as experience changes in calcification rates, in response to OA and/or warming. These findings contribute to a better understanding of calcification dynamics in CCA through the mechanistic exploration of organic matrix modulation under OA and warming.

MATERIALS AND METHODS

Sample collection and study area. Lizard Island, northern Great Barrier Reef (GBR; 14°41′17.4″ S 145°28′03.6″ E & 14°41′47.0″ S 145°27′02.9″ E) was chosen as the study site for its accessible lagoonal reefs, which are composed of an abundant and diverse CCA community (E. Bergstrom and G. Diaz-Pulido, pers. obs.). Additionally, the northern third of the GBR has experienced substantial loss of coral cover over the past decades due to successive coral bleaching events, crown of thorns starfish outbreaks, and cyclones, where >50% of corals in shallow habitats died in 2016 alone (Tarte and Hughes 2020). Thus, under these circumstances there is an increasing amount of dead coral that provides opportune substrate for CCA to settle, grow, and consolidate the reef.

The following four species were selected for this study in order to assess cell wall matrix composition variability across CCA: *Porolithon* cf. *onkodes* (orange morph), *Lithophyllum* cf. *insipidum*, *Lithothamnion proliferum*, and *Sporolithon* cf. *durum*. The species identity of all specimens was verified via morphological examination under a dissecting microscope and selected specimens were examined anatomically under a compound microscope according to the following taxonomic resources: Gordon et al. 1976, Adey et al. 1982, Ringeltaube and Harvey 2000, and Kato et al. 2011, among others (for further species identification methods, see Appendix S1 in the Supporting Information). These species are common reef builders, abundant throughout the GBR (Dean et al. 2015) and the Indo-Pacific region (Adey et al. 1982), and they represent three of the four existing CCA lineages: Corallinales, Hapalidiales, and Sporolithales (fourth: Corallinapetrales; Peña et al. 2020, Jeong et al. 2021). Fragments of approximately 6 cm^2 from each species were removed from the reef using hammer and chisel. *Porolithon* cf. *onkodes* and *L.* cf. *insipidum* commonly occur at 2 m where mean incident irradiance is 314 ± 22 SE μmol photons · m^{-2} · s^{-1} (LI-COR LI-1500 light sensor logger coupled to an LI-193SA underwater spherical quantum sensor), and *L. proliferum* and *S.* cf. *durum*

at 6 m where it is 44 ± 7 SE μmol photons · m^{-2} · s^{-1}, as their corresponding lineages have evolved to occupy high and low light environments, respectively (Aguirre et al. 2000). Fragments were brought back to the outdoor aquarium facility at Lizard Island Research Station (LIRS) to acclimatize at ambient seawater temperature and pCO$_2$ for one week.

Collected fragments were subsequently removed of unnecessary substrate and visible endobionts, and a thin layer of Coral Glue® (EcoTech Marine) was spread across exposed calcium carbonate underneath the fragments so as to minimize changes in fragment weight that are not related to the metabolic processes of the algae (e.g., dissolution of loose CaCO$_3$).

Experimental design. To test the effects of OA and warming on the composition of the CCA cell wall matrix, a manipulative tank experiment was conducted that employed a full factorial design of an ambient and an elevated level of both seawater temperature (27.2 and 29.4°C) and pCO$_2$ (465 and 1025 μatm), totaling 4 treatment combinations, each with five replicates (20 experimental tanks). This experiment was conducted in a flow-through mesocosm system at LIRS from the end of austral spring to summer (October–December), 2018. One CCA fragment per species was placed in each experimental tank and these were subjected to treatments for 2 months, with the exception of *Lithophyllum* cf. *insipidum*, which was removed at 1 month due to health decline (paling of surficial pigmented tissue) in fragments across all treatments. Further details of the ocean acidification and warming experiment and a description of the seawater carbonate chemistry analyses conducted in this study can be found in Appendix S1.

Light levels of approximately 30 and 250 μmol photons · m^{-2} · s^{-1} were targeted for low- and high-light CCA, respectively. Shade cloth was placed on the top (to reduce incident light) and bottom (to limit reflection) of one half of each experimental tank where low-light species were situated. The other side was kept uncovered for the high-light species. Photosynthetically active radiation (PAR) was measured at various times of the day on both sides of the experimental tanks. PAR on the shaded side measured 20 at 9:00, 65 at 12:00 and 20 at 17:00 (μmol photons · m^{-2} · s^{-1}). The unshaded side measured 100 at 9:00, 220 at 12:00, and 100 at 17:00 (μmol photons · m^{-2} · s^{-1}).

Post-experimentation, fragments were cleaned of surficial epiphytes, dried at 60°C for 24 h and stored in silica desiccant, transported to Griffith University (Nathan) for processing and inorganic carbon content analysis, and then transported to the University of Adelaide for monosaccharide analysis (see below).

Cell wall carbohydrate analysis. Algal sample preparation: To characterize cell wall organic matrix composition across species and treatments, the surficial organic algal tissue of experimental fragments was isolated according to Bergstrom et al. (2020). Field and experimental tank CCA fragments were decalcified in 10% aqueous HCl for approximately 1.5 min. The fragments were rinsed immediately in deionized (DI) water to remove any debris and the decalcified surficial cell layers were scraped off using a sterile razor blade under a dissecting microscope (Olympus SZX16), targeting only the surficial, pigmented cell layers. This corresponds to new cells produced during experimentation (i.e., approximately 15–80 μm into the crust). This range of surficial cell growth was determined by Bergstrom et al. (2020) via calcein staining and microscope observations performed on the same species under nearly identical treatment conditions. Algal tissue was placed on a 47 mm Whatman GF/F filter, rinsed five times with DI water and dried overnight at 60°C. Samples were ball milled in 2-mL polypropylene tubes for 30 s at 30 Hz using a Retsch Mill MM400.

Alcohol-insoluble residue (AIR) preparation, hydrolysis and derivatization: To prepare the alcohol-insoluble residue comprising organic matrices, ground material was extracted twice with 70% aqueous ethanol on a slow rotor at room temperature for 15 min, then once each with ethanol and acetone, followed by drying in a desiccator.

Monosaccharide analysis: Technical duplicates were produced for each sample by weighing approximately 0.5 mg of algal AIR samples into Eppendorf tubes and hydrolyzed with 100 µL 2 M trifluoroacetic acid (TFA) at 100°C for 3 h. After cooling to room temperature, the hydrolysates were dried in a centrifugal evaporator, re-suspended in 50 µL methanol, dried again, and finally dissolved in water. The resulting solutions were analyzed for monosaccharide content (type and relative abundance) essentially as described in Little et al. (2019). Carbohydrates in appropriately diluted hydrolysates (10 µL) were derivatized with 1-phenyl-3-methyl-5-pyrazolone (PMP) along with the same volume of a suitable set of calibration standards. 2-Deoxy-ribose was used as the internal standard and the solutions of derivatives were analyzed using reversed phase High-Performance Liquid Chromatography (HPLC) on an Agilent 1260 liquid chromatography (LC) system. 10 µL of each derivative solution was injected onto a Phenomenex Kinetex C18 column (dimension: 100 × 3 mm; particle size 2.6 µm; porosity 100 Å), operated at a flow rate of 0.8 mL·min^{-1} and 30°C. The eluents used were (A) 10% acetonitrile, 40 mM ammonium acetate (pH 6.8), (B) 70% acetonitrile, and (C) 40 mM acetic acid. The gradient was 8 to 17% (B) over 9.3 min with (A), and then flushed for 1 min with 90% (B)/10% (C) before re-equilibrating to start conditions. The monosaccharide derivatives were detected by measuring the absorbance at 250 nm. The concentrations of the following monosaccharides were determined by comparison of the corresponding peak areas on the LC chromatograms to standard curves of calibrants: D-guluronic acid (GulA), D-mannuronic acid (ManA), D-mannose (Man), L-ribose (LRib), D-glucosamine (GlcN), D-glucuronic acid (GlcA), D-galacturonic acid (GalA), D-glucose (Glc), D-galactose (Gal), D-xylose (Xyl), L-arabinose (LAra), L-fucose (LFuc), and unidentified peaks (UNI) B – G. UNI-A was identified as GlcN and for all further analysis GlcN was included as a calibrant. Unidentified peaks were arbitrarily quantified as xylose equivalents as the extinction coefficients of monosaccharide PMP derivatives at 250 nm do not vary significantly. L-Galactose (LGal) was not quantified. It is found to be present in a 1:1.05 ratio to D-galactose in the calcified intergenicula of a coralline alga (Martone et al. 2010), and thus, results should be interpreted with this in mind. The concentrations of all discrete monosaccharides present in each sample were summed and the relative abundance of each monosaccharide (expressed as mol%) was calculated by dividing its individual concentration by the total concentration of all monosaccharides. SXGs are characterized by their ratio of Gal to Xyl (Usov et al. 1995, Navarro et al. 2011). To gauge insights into the presence of SXGs, the D-galactose:D-xylose ratio was calculated by dividing the relative abundance of the former monosaccharide by that of the latter.

Characterization of unidentified monosaccharides: Fractions containing PMP derivatives that did not co-elute with calibration standards were manually collected, desalted using C-18 Solid Phase Extraction (SPE), and analyzed using Liquid Chromatography-Mass Spectrometry (LC-MS^2) on an Agilent 1290 LC system coupled to an Agilent 6545 quadrupole time of flight (qTOF) mass spectrometer (Agilent Technologies, Singapore; Little et al. 2019).

Surficial inorganic carbon content. To determine the calcification rate of the surficial thallus, we quantified the surficial inorganic carbon content by isolating the inorganic skeleton from the organic tissue in only the photosynthetic cell layers. A 1-cm^2 surface area of surficial, pigmented tissue was uniformly dry-scraped with a sterile razor blade from a different individual fragment than those used for monosaccharide analyses of the same species for each tank. The powder was placed in a tin tray and samples were ignited in a muffle furnace (Lenton ECF12/4) at 550°C for 3 h to remove all organic tissue, leaving only CaCO$_3$, according to the Loss-On-Ignition Method (Dean 1974). Isolated inorganic skeleton (i.e., CaCO$_3$) was then pre-weighed into separate tin capsules, pelleted, and analyzed for carbon content (C_{inorg}, µg) using an Elemental Analyzer (Europa EA-GSL) coupled to an Isotope ratio Mass Spectrometer (Sercon Hydra 20–22) calibrated to certified reference material (IAEA-CH-6 Sucrose, Australian National University, Canberra). To normalize measurements to a proxy for biomass, the surface area of fragments was calculated using the aluminum foil technique (Marsh Jr 1970).

Net calcification. To better understand the role and relevance of the relationship between organic matrix dynamics and biomineralization in the CCA crust, net calcification rates of the whole thallus were quantified using the buoyant weight method (Langdon et al. 2010). Individual live fragments were weighed at the beginning and at the end of the experiment and net calcification was calculated using the following sequential equations:

$$\Delta W_a = \frac{(W_{wf} - W_{wi})}{SA\left(1 - \frac{\rho_w}{\rho_s}\right)} \quad (1)$$

where ΔW_a is the change in dry weight of the CCA fragment from initial to final measurement, W_{wf} is the final buoyant weight, W_{wi} is the initial buoyant weight, ρ_w is the density of seawater (1.023 g · cm^{-3}), ρ_s is the density of skeletal material (calcite, 2.71 g · cm^{-3}), and SA is the surface area.

$$G = \frac{\Delta W_a}{\Delta t} \quad (2)$$

where G is the net calcification rate (mg CaCO$_3$ cm^{-2} d^{-1}), ΔW_a is the change in dry weight of the CCA fragment from initial to final measurement, and Δt is the change in time between initial and final measurements (expressed in days).

Statistical analyses. To assess the dissimilarity of cell wall monosaccharide composition across treatments in the four species, a multidimensional scaling (MDS) ordination analysis was performed with the Bray Curtis dissimilarity metric using the vegan package (Oksanen et al. 2019). Data were square root-transformed to reduce the influence of extreme values on ordination. To test the effects of pCO$_2$ and temperature on monosaccharide relative abundance, the galactose:xylose ratio, net calcification, and surficial C_{inorg} content across the four species of CCA, we used two-way Analyses of Variance (ANOVAs) with pCO$_2$ (two levels) and temperature (two levels) as fixed factors and tanks as replicates. Two-way ANOVAs were conducted for each species separately. Outliers were removed, resulting in $n = 4–5$ across treatments. Normality and equality of variance assumptions were evaluated via graphical analysis of residuals. For some response variables the data were log-transformed to meet these assumptions. So as to not overpower the effects of pCO$_2$ and temperature on the other less abundant monosaccharides, glucose was excluded from the mol % calculation for the ANOVA analyses, and thus, its data were analyzed as concentrations (µM). Mol % values were recalculated for the remaining monosaccharides to exclude the relative abundance of glucose. ANOVAs were followed by Tukey's HSD post hoc pairwise comparisons when a significant interaction was detected

between pCO$_2$ and temperature. Otherwise, a t-test or one-way ANOVA was run if there was a significant effect of only one variable. To assess the relationship between ambient surficial C_{inorg} content and net (whole-thallus) calcification, a linear regression analysis was performed. All analyses were performed in R v3.5.1.

RESULTS

Cell wall carbohydrate composition. There was a distinct separation between matrix monosaccharide compositions across CCA species (Fig. 1; MDS stress = 0.048). *Porolithon* cf. *onkodes* and *Lithophyllum* cf. *insipidum* were the most similar in composition, whereas *Sporolithon* cf. *durum* and *Lithothamnion proliferum* appear to be equally dissimilar to each other and to the other two species (Fig. 1). Glc residues were the dominant constituent in the cell walls of all but *S.* cf. *durum*, ranging from 25–74% of total monosaccharides (Fig. 2). In *S.* cf. *durum* and *L. proliferum*, Glc residues comprised <50% of monosaccharides, and in *P.* cf. *onkodes* and *L.* cf. *insipidum*, they comprised >50% (Fig. 2). *Porolithon* cf. *onkodes* had the highest abundance of GulA and ManA residues, *S.* cf. *durum* had the highest abundance of Man residues (its most abundant constituent), and *L. proliferum* (24.5%) and *S.* cf. *durum* (25.5%) had higher abundances of Gal residues than *P.* cf. *onkodes* (7.8%) and *L.* cf. *insipidum* (11.4%; Fig. 2). In addition, ratios of galactose:xylose spanned a large range across species, varying from 2.5–11:1 (Fig. 3).

Characterization of unidentified monosaccharides. High-resolution mass analysis of peaks eluting at retention times of known standards showed masses consistent with PMP derivatives of the corresponding monosaccharides (data not shown). Analysis of the unidentified peaks (D, E, F, G; Fig. 4a) gave fragmentation patterns with dominant m/z signals of 175.09 and 373.17, consistent with molecular ions of PMP-methyl-hexosyl derivatives, within a 10-ppm variation range (Fig. 4b). These are possibly methylated Gal residues (Usov 2011). Unidentified peak E was seen to split into two peaks under the LC conditions used for this analysis; both these peaks showed the same molecular ion as D, F, and G. We were unable to identify peaks B and C due to low sample quantities.

Shifts in carbohydrates under OA and warming. When excluding Glc, total monosaccharide concentration did not significantly change across treatments (Table S1 in the Supporting Information), except in *Lithophyllum* cf. *insipidum*, where a main temperature effect resulted in a greater total concentration at elevated temperature than ambient temperature, regardless of pCO$_2$ (two-way ANOVA, main pCO$_2$ effect, $F_{1,16} = 7.04$, $p = 0.017$; Table S2 in the Supporting Information). Monosaccharide richness was also largely unaffected by treatments across species (Table S1). Investigations into the relative abundances of individual matrix components, however, showed different responses across CCA taxa to pCO$_2$ and temperature stress (Tables 1, S1, S3 in the Supporting Information, two-way ANOVA). For all species, either pCO$_2$ or temperature had a significant effect on Glc concentration (Fig. 5). In *Porolithon* cf.
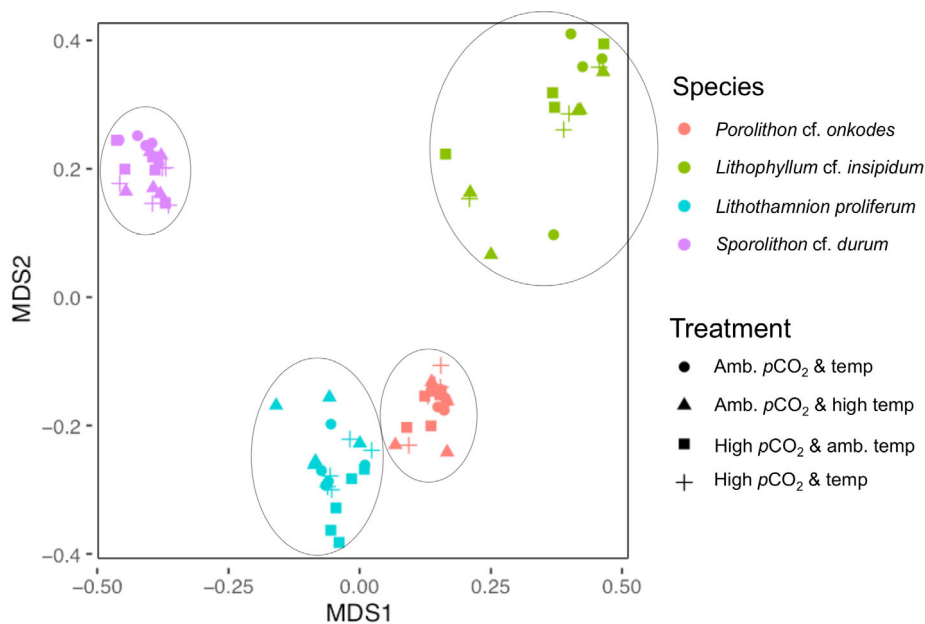

Fig. 1. Multidimensional scaling (MDS) ordination plot illustrating the dissimilarity (Bray Curtis) of the monosaccharide composition of polysaccharides across CCA species exposed to seawater pCO$_2$ and temperature treatments (465 µatm and 27.2°C, 465 µatm and 29.4°C, 1160 µatm and 27.2°C, 1160 µatm and 29.4°C). *Lithophyllum* cf. *insipidum* (upper right-hand cluster), *Lithothamnion proliferum* (lower left-hand cluster), *Porolithon* cf. *onkodes* (lower right-hand cluster), and *Sporolithon* cf. *durum* (upper left-hand cluster; stress = 0.048). [Color figure can be viewed at wileyonlinelibrary.com]
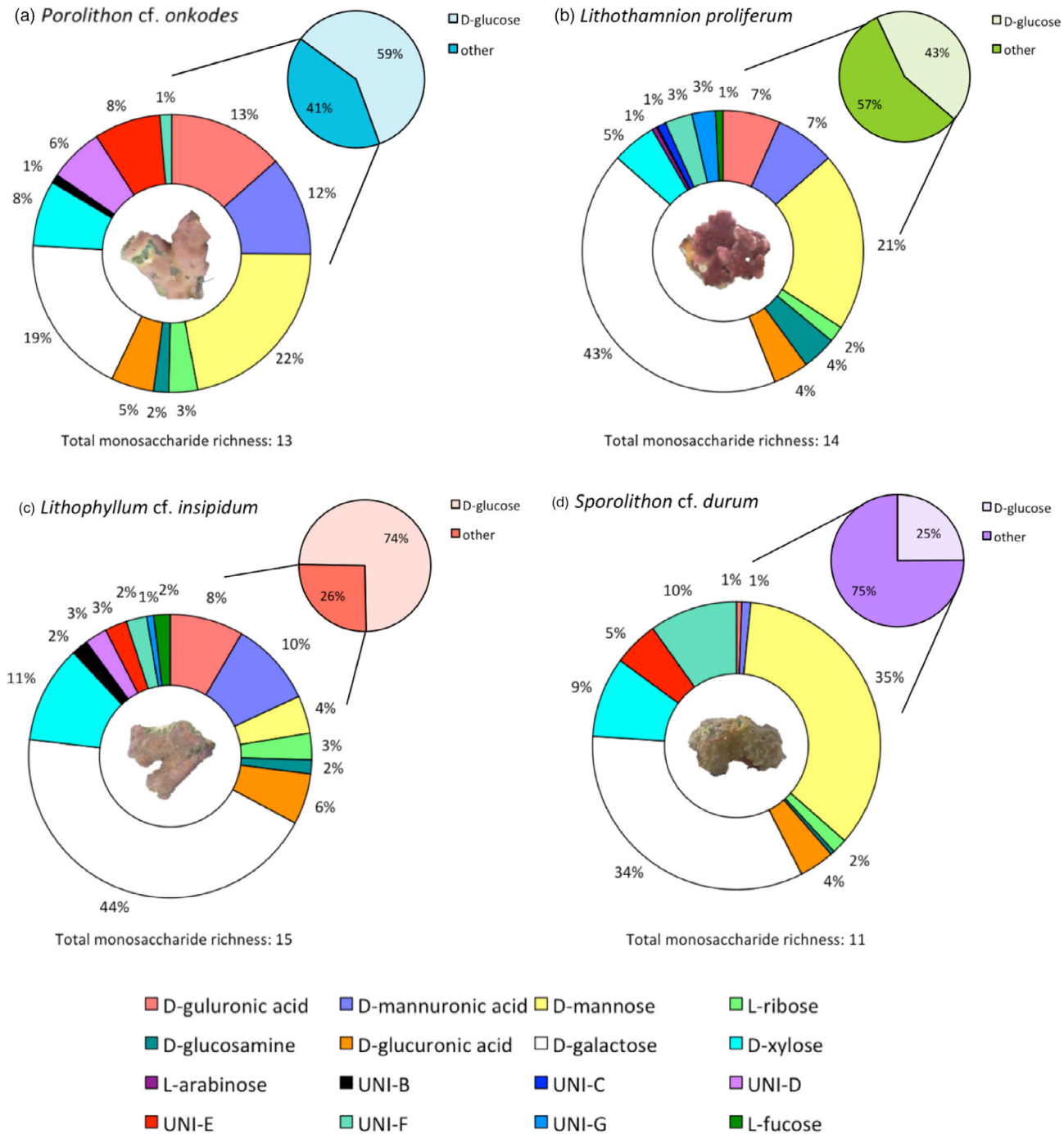
FIG. 2. Ambient cell wall monosaccharide composition of the crustose coralline algae (a) *Porolithon* cf. *onkodes*, (b) *Lithothamnion proliferum*, (c) *Lithophyllum* cf. *insipidum*, and (d) *Sporolithon* cf. *durum*. Pie charts depict relative abundance (mean mol% $\pm$ SE) of glucose compared to other monosaccharide constituents. Doughnut charts represent relative abundances of non-glucosidic constituents, having excluded glucose from the abundance calculation, i.e., percentages in doughnut chart = 100% instead of the indicated "other" percent in the pie chart. All constituents with abundances <1% are considered negligible and are not labeled ($n = 5$). UNI signifies unidentified monosaccharide peaks that classify as methylated galactosyl residues (except UNI-B, which remains uncharacterized).

onkodes and *Sporolithon* cf. *durum,* a pCO_2 effect was observed (two-way ANOVA, main pCO_2 effect, $F_{1,16} = 5.36$, $P = 0.034$; $F_{1,16} = 6.01$, $P = 0.026$, respectively), resulting in 52 and 72% more Glc, respectively, under elevated pCO_2 than ambient pCO_2, regardless

of temperature (Fig. 5, a and d). For *Lithothamnion proliferum* and *L.* cf. *insipidum*, a temperature effect was observed (two-way ANOVA main temp effect, $F_{1,13} = 14.51$, $P = 0.002$; $F_{1,16} = 7.31$, $P = 0.016$, respectively), resulting in 89 and 54% more Glc, respectively,
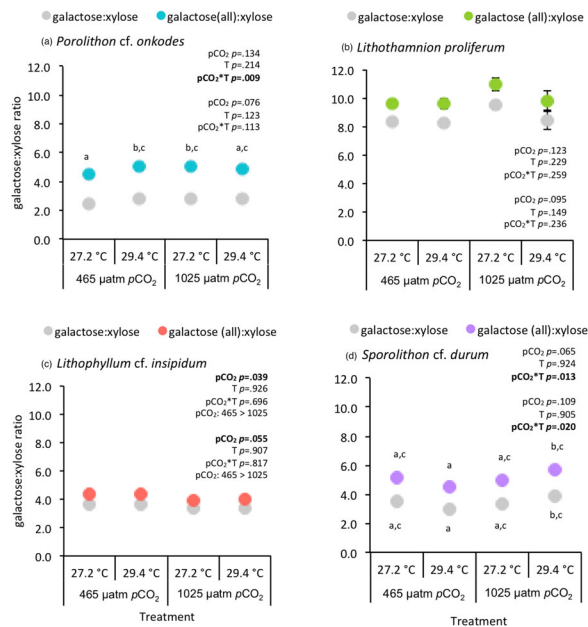
FIG. 3. Responses of the ratio of galactose:xylose and galactose:xylose (all; i.e., galactose + all unidentified methylated galactosyl residues) to the full factorial combination of ambient (465 µatm) and elevated (1160 µatm) pCO_2 and ambient (27.2°C) and elevated temperature in (a) *Porolithon* cf. *onkodes* ($n = 5$), (b) *Lithothamnion proliferum* ($n = 4$–5), (c) *Lithophyllum* cf. *insipidum* ($n = 4$–5), and (d) *Sporolithon* cf. *durum* ($n = 5$). Values are means $\pm$ SE. Significant differences ($P < 0.050$) between treatments resulting from Tukey HSD post hoc pairwise comparisons are indicated by unalike lowercase letters. [Color figure can be viewed at wileyonlinelibrary.com]

under elevated temperature than ambient temperature, regardless of pCO_2 (Fig. 5, b and c).

Much smaller shifts in the less abundant monosaccharides were observed in response to pCO_2 and temperature (Table S3). In *Porolithon* cf. *onkodes*, elevated pCO_2 and temperature often affected monosaccharide abundances (mol %) in opposite directions (Table S1). Within observed interactive pCO_2/temp effects, elevated pCO_2 at ambient temperature resulted in increased GulA and UNI-B in *P.* cf. *onkodes*, while it also led to decreased Xyl. Also, in *P.* cf. *onkodes*, a main temperature effect resulted in decreased Man at elevated temperature (Tables S1, S3). For *Lithophyllum* cf. *insipidum*, the sole elevation of temperature resulted in increased UNI-B, while Xyl increased under elevated pCO_2, regardless of temperature (two-way ANOVA, $F_{1,8} = 6.01$, $P = 0.028$; $F_{1,16} = 14.59$, $P = 0.002$, respectively). In *L. proliferum*, there was an antagonistic interactive effect of pCO_2 and temperature on GulA and UNI-C (two-way ANOVA, interaction pCO_2 x temp, $F_{1,13} = 8.06$, $P = 0.015$; $F_{1,8} = 7.03$, $P = 0.029$, respectively), where elevated temperature largely resulted in either an increase or decrease in abundance that pCO_2 ultimately ameliorated. Unidentified monosaccharide peaks (i.e., UNIs) aligned most closely with methylated hexosyl

residues and were treated as such in interpretations (except UNI-B, which remains unidentified; Fig. 4). In *Sporolithon* cf. *durum*, interactive effects of pCO_2 and temperature were present for Man, LRib, GlcA, and Xyl (two-way ANOVA, interaction $pCO_2 \times$ temp, $F_{1,15} = 6.87$, $P = 0.019$; $F_{1,15} = 6.09$, $P = 0.026$; $F_{1,16} = 6.03$, $P = 0.026$; $F_{1,16} = 5.37$, $P = 0.034$, respectively). Elevated temperature largely resulted in an increased abundance of LRib, GlcA, and Xyl and a decreased abundance of Man, which were ultimately mitigated by elevated pCO_2 (Table S1).

The galactose:xylose ratio responses to pCO_2 and temperature differed marginally across species (Table S3). In *Porolithon* cf. *onkodes*, when considering the unidentified (i.e., UNI) monosaccharides as Gal residues (except UNI-B), an interactive effect resulted in increased galactose (all):xylose ratios under the sole elevation of pCO_2 or temperature (Fig. 3a, two-way ANOVA interaction $pCO_2 \times$ temp, $F_{1,16} = 8.88$, $P = 0.009$). No effect was observed for *Lithothamnion proliferum* (Fig. 3b). In *Lithophyllum* cf. *insipidum*, there was a trend of decreased galactose:xylose ratios, regardless of the inclusion or not of the unidentified peaks, under elevated pCO_2, regardless of temperature (Fig. 3c, two-way ANOVA, main pCO_2 effect, $F_{1,15} = 5.10$, $P = 0.039$; $F_{1,15} = 4.31$, $P = 0.055$, respectively). In *Sporolithon* cf. *durum*, there was an antagonistic interaction, regardless of the inclusion or not of the unidentified peaks, where galactose:xylose ratios decreased under elevated temperature, but the effect was mitigated by elevated pCO_2 (Fig. 3d, two-way ANOVA, interaction $pCO_2 \times$ temp, $F_{1,16} = 7.77$, $P = 0.013$; $F_{1,16} = 6.63$, $P = 0.020$, respectively).

Surficial and whole-thallus calcification. Surficial calcification measured as inorganic carbon content was significantly affected by elevated pCO_2 and/or temperature in all CCA, but the nature of the effect differed across species (Table S4 in the Supporting Information). *Porolithon* cf. *onkodes* was the only species to decrease surficial C_{inorg} content under elevated pCO_2 due to a main pCO_2 effect (Fig. 6a, two-way ANOVA, $F_{1,14} = 8.64$, $P = 0.011$). In *Lithophyllum* cf. *insipidum*, *Sporolithon* cf. *durum*, and *Lithothamnion proliferum*, there were antagonistic interactions. In the former two, the antagonistic interaction resulted in increased surficial C_{inorg} content at elevated temperature, which was reversed by elevated pCO_2 (Fig. 6, c and g, two-way ANOVA, interaction $pCO_2 \times$ temp, $F_{1,13} = 5.17$, $P = 0.041$; $F_{1,12} = 9.00$, $P = 0.011$, respectively). In the latter species, the antagonistic interaction resulted in increased surficial C_{inorg} content at elevated pCO_2, which was reversed by elevated temperature (Fig. 6e, two-way ANOVA, interaction $pCO_2 \times$ temp, $F_{1,14} = 12.62$, $P = 0.003$). There was no significant correlation between the net calcification response and surficial inorganic carbon content response for any species (Fig. S1 in the Supporting Information, LM, all $P > 0.05$).
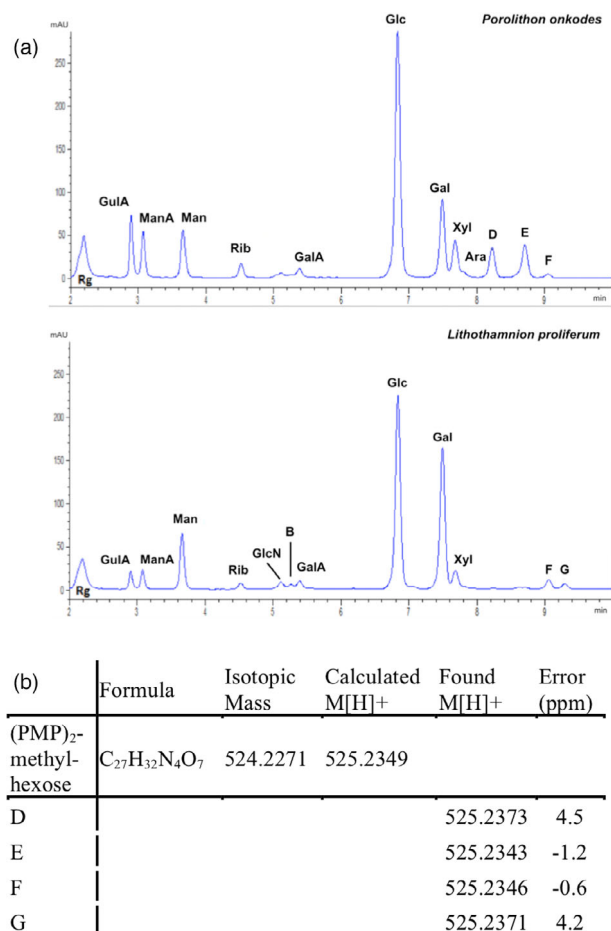
FIG. 4. HPLC analysis of crustose coralline algae. (a) Chromatograms of acid hydrolyzed and PMP-derivatized samples of *Lithothamnion proliferum* and *Porolithon* cf. *onkodes* showing the unidentified peaks D, E, F and G. (b) LC-MS2 analysis of unidentified peaks collected from HPLC analysis. Masses are consistent with PMP derivatives of methylated hexoses and fragmentation patterns are consistent with those of known PMP-standards. Abbreviations: Rg, reagent; GulA, guluronic acid; ManA, mannuronic acid; Man, mannose; Rib, ribose; GlcN, glucosamine; GalA, galacturonic acid; Glc, glucose; Gal, galactose; Xyl, xylose; Ara, arabinose. [Color figure can be viewed at wileyonlinelibrary.com]

Whole-thallus net calcification rates (via buoyant weight) were differentially affected by pCO$_2$ and temperature across CCA taxa (Fig. 6, Table S4). *Lithothamnion proliferum* had no significant change in net calcification across treatments (Fig. 6f). In contrast, *Lithophyllum* cf. *insipidum* displayed decreased net calcification under elevated pCO$_2$, regardless of temperature (Fig. 6d, two-way ANOVA, main pCO$_2$ effect, $F_{1,15} = 12.07$, $P = 0.003$). The response of *Porolithon* cf. *onkodes* was similar to *L.* cf. *insipidum*, but the decrease was not significant due to within-pCO$_2$ treatment variability (Fig. 6b, two-way ANOVA, pCO$_2$, $F_{1,14} = 2.22$, $P > 0.05$). For *Sporolithon* cf. *durum*, a non-additive interaction resulted in significantly lower net calcification at elevated pCO$_2$ and

temperature than the control (Fig. 6h, two-way ANOVA, interaction pCO$_2$ × temp, $F_{1,13} = 18.36$, $P = 0.001$).

DISCUSSION

Organic matrix composition differed across the four CCA species tested from mid-shelf GBR communities, which indicated variability in the polysaccharides present, and thus, the properties of their organic matrices. We also establish for the first time that CCA have the ability to modulate monosaccharide abundances to varying degrees under OA and warming. *Porolithon* cf. *onkodes* was the only species whose change in the monosaccharide composition of polysaccharides occurred alongside a decline in surficial calcification, whereas the changes in composition in *Lithophyllum* cf. *insipidum*, *Sporolithon* cf. *durum*, and *Lithothamnion proliferum* were associated with maintained or even marginally increased surficial calcification. Our findings of variable calcification responses and modulation of organic matrix carbohydrates highlight implications of the different structural and inducing components of organic matrices across species and environmental scenarios that enhance our understanding of biomineralization in CCA.

Variability in organic matrix constituents across CCA species. Dissimilarity among species' monosaccharide constituents suggests that different polysaccharides compose organic matrices across CCA taxa. The types of monosaccharide residues present, as well as the relative ratios of particular monosaccharides, can be indicative of the matrix component they comprise in the cell wall. Our results show that Glc was the most abundant sugar in matrix polysaccharides in *Porolithon* cf. *onkodes*, *Lithophyllum* cf. *insipidum*, and *Lithothamnion proliferum*. Previous linkage analyses of the Glc residues present in an α-amylase-treated (i.e., no starch present) articulate coralline identified them as 4-linked Glc. In corallines, 4-linked Glc residues likely arise from cellulose (Martone et al. 2019) or α-glucans (i.e., floridean starch; Al Abdallah et al. 2016). However, starch is largely stored intracellularly (i.e., in the cytosol) in red algae (Pueschel 1990, Viola et al. 2001) and any cell wall α-glucans would likely be soluble as their mean chain length is in the range 9–17 (Turvey and Simpson 1966, Ozaki et al. 1967). Thus, we predict that our insoluble Glc residues largely arise from cellulose, a common microfibrillar skeletal component in macroalgae (Frei and Preston 1961, Usov 1992, Tsekos 1999, Vreeland and Kloareg 2000, Lee 2018), particularly in the secondary cell walls of corallines (Martone et al. 2019). It still must be confirmed through further research whether most cellulose present in the cell walls of CCA is microfibrillar (CMFs). The lower percentage of Glc in *Sporolithon* cf. *durum* may suggest fewer or shorter cellulose chains.

TABLE 1. Summary of the effects of temperature and pCO_2 on the monosaccharides in the cell wall organic matrices of *Porolithon* cf. *onkodes*, *Lithothamnion proliferum*, *Lithophyllum* cf. *insipidum*, and *Sporolithon* cf. *durum*.

Species	Monosaccharide	Temperature effect	pCO_2 effect	Interactive effect
Porolithon cf. *onkodes*	Glc		52%↑	
	GulA			High pCO_2 40%↑
	UNI-B			High pCO_2 231%↑
	Xyl			High pCO_2 22%↓
	Man	16%↓		
	Gal(all):Xyl			High temp 12%↑, high pCO_2 13%↑
	Surficial C_{inorg}		19%↓	
Lithothamnion proliferum	Glc	89%↑		
	GulA			No pairwise significance
	UNI-C			No pairwise significance
	Surficial C_{inorg}			High pCO_2 38%↑
Lithophyllum cf. *insipidum*	Glc	54%↑		
	UNI-B	30%↑		
	Xyl		9%↑	
	Gal:Xyl		7%↓*	
	Gal(all):Xyl		8%↓	
	Surficial C_{inorg}			High temp 71%↑
	Whole-thallus calcification		88%↓	
Sporolithon cf. *durum*	Glc		72%↑	
	Man			No pairwise significance
	LRib			No pairwise significance
	GlcA			No pairwise significance
	Xyl			No pairwise significance
	Gal:Xyl			*High temp&pCO₂ 29% > high temp*
	Gal(all):Xyl			*High temp&pCO₂ 26% > high temp*
	Surficial C_{inorg}			High temp 44%↑
	Whole-thallus calcification			High temp 51%↓, High pCO_2 57%↓, High temp&pCO_2 42%↓

Values indicate the magnitude of change (%) from ambient conditions (except italicized results) and the arrows indicate the direction.
*Indicates a nearly significant trend.

Moreover, after Glc, Man and Gal residues are among the most abundant constituents of coralline cell wall polysaccharides. The latter typically indicates the presence of galactans in coralline algae (Navarro and Stortz 2008, Navarro et al. 2011). Our findings of higher abundances of Gal residues in *Lithothamnion proliferum* and *Sporolithon* cf. *durum* than *Lithophyllum* cf. *insipidum* and *Porolithon* cf. *onkodes* suggest that the former species' organic matrices may possess a relatively greater portion of galactans. Regarding galactose:xylose ratios, although that of *P.* cf. *onkodes* is currently most indicative of SXG presence (close to 2.3:1; Usov et al. 1995), further analyses would be required to quantify LGal and ascertain UNI residue identities to determine how their presence impacts the ratio across species. In addition, Man residues typically form the backbone of linear β-(1 → 4)-mannans, which can form microfibrils in fleshy rhodophytes (Rodríguez-Gacio et al. 2012). Mannans are also found in the cell walls of calcified red algae, *Galaxaura squalida* and *Liagora valida* (Stiger-Pouvreau et al. 2016). Although mannans are not yet reported in corallines (Martone et al. 2010), the Man yield and linkage type previously reported for *Lithothamnion heterocladum* suggested the presence of 4-linked mannans and Man-containing heteropolysaccharides

in the cell wall (Navarro et al. 2011). Considering this, our findings of the highest abundance of Man in *S.* cf. *durum* (Man also being the most abundant sugar in its matrix polysaccharides), could suggest that mannans and other heteropolysaccharides are relatively more abundant in the organic matrix of this species. Linkage analyses would be required to characterize the ratio of mannan and/or Man-containing heteropolysaccharides, as well as to assess their ability to form microfibrils. This is however challenged by the difficulty of isolating sufficient quantities of these polymers in crustose coralline algae.

Differential abundance of GulA and ManA residues across taxa could indicate differences in polyuronide presence. These residues are the only monomers of alginates (Okazaki et al. 1982, Bilan and Usov 2001, Navarro et al. 2011), which are a polymeric systemic marker of Corallinaceae (Bilan and Usov 2001). We found the highest abundances of GulA and ManA residues in *Porolithon* cf. *onkodes*, suggesting a relatively higher abundance of alginates in the organic matrix of this species. Continued discoveries of cell wall polysaccharide and glycoprotein structure and identity (e.g., Martone et al. 2009, 2010, Rahman and Halfar 2014, Rahman et al. 2019), as well as variability in metabolomic
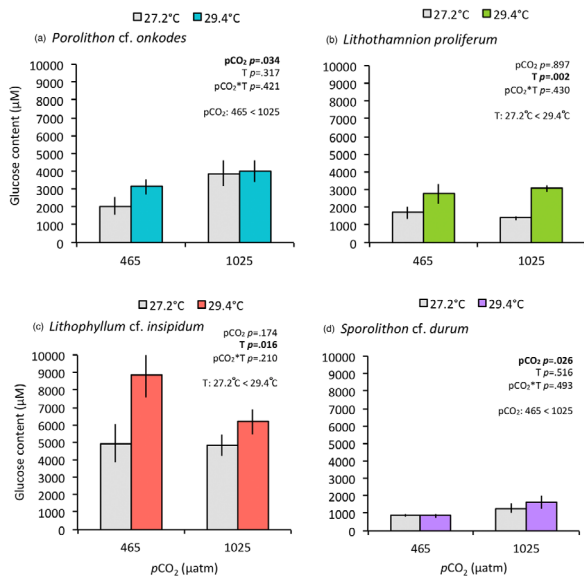
ELLIE BERGSTROM ET AL.

FIG. 5. Responses of D-glucose content (μM) of the alcohol insoluble fraction to the full factorial combination of ambient (465 μatm) and elevated (1160 μatm) pCO_2 and ambient (27.2°C) and elevated temperature (29.4°C) in (a) *Porolithon* cf. *onkodes*, (b) *Lithothamnion proliferum*, (c) *Lithophyllum* cf. *insipidum*, and (d) *Sporolithon* cf. *durum*. Values are means ± SE of $n = 5$. [Color figure can be viewed at wileyonlinelibrary.com]

profiles (Jorissen et al. 2021), will likely result in a refined understanding of matrix composition and biomineralization in coralline algae.

Potential implications of organic matrix composition for biomineralization. There are various implications for biomineralization based on the different structural and inducing properties of the observed constituents across CCA taxa. Mannans, cellulose, and other polymers form physically different structures (Kloareg and Quatrano 1988). Depending on the monomer configuration, mannans can form dimers and two-fold helical structures, whereas cellulose forms ribbon-like structures (Stiger-Pouvreau et al. 2016). The comparatively higher abundance of the monomer that is characteristic of mannans in *Sporolithon* cf. *durum* could implicate different structural properties of the matrix than the other species. Additionally, the comparatively greater presence of cellulose, that is predicted to form CMFs, in the cell walls of *Porolithon* cf. *onkodes* and *Lithophyllum* cf. *insipidum* could play a role in biomineralization. CMFs are proposed to be the substrate that is crystallized when surrounded by inducing polysaccharides (Lowenstam 1981, Borowitzka and Larkum 1987, Nash et al. 2019), however, cellulose abundance alone has not been implicated in biomineralization, and it is well known that cellulose is present in the cell walls of many other species of non-calcifying red algae (Siegel and Siegel 1973). In the articulated coralline, *Calliarthron* sp., cellulose comprised the same percentage of algal wet weight in genicula as it did in

decalcified intergenicula (Martone et al. 2019, Janot et al. 2022). Thus, biomineralization would likely also depend on the abundance of inducing polysaccharides.

Alginates are shown to be involved in the biomineralization of corallines (Okazaki et al. 1982, Navarro et al. 2011) due to their good scaffold-forming property (Venkatesan et al. 2015) and high affinity for bivalent cations, particularly calcium (Rees and Welsh 1977, Bilan and Usov 2001). Due to their gel-forming properties, it is logical that alginates likely occupy the matrix fluid of coralline cell walls alongside other polymers (Venkatesan et al. 2015, Nash et al. 2019). The relatively high ambient abundance of monomers characteristic of alginates in *Porolithon* cf. *onkodes* may be indicative of a strategy of compensating for the large quantity of cellulose to achieve biomineralization. Furthermore, galactans are also recognized for their gelling properties across red seaweeds, and are classified as agarans or carrageenans depending on their stereochemistry (Stortz and Cerezo 2000). Particular SXGs are unique to corallines and are recognized as matrix fluid inducing polysaccharides (Cases et al. 1994, Navarro and Stortz 2008, Martone et al. 2010). The suggested higher relative abundance of monomers characteristic of galactans in *Lithothamnion proliferum* and *Sporolithon* cf. *durum* than *P.* cf. *onkodes* and *Lithophyllum* cf. *insipidum* could differentially affect the properties of the organic matrix between the former and latter species depending on the galactan substituents (Ferreira et al. 2012). Continued research into the comparative presence of SXGs would shed light on the biomineralization mechanisms of these species.

Organic matrix modulation under OA and warming and implications for biomineralization. In agreement with our hypothesis, shifts in monosaccharide constituent abundance varied under elevated pCO_2 and/or temperature across taxa, suggesting that CCA are differentially capable of modulating the abundance of discrete cell wall constituents. Based on the properties of the shifting constituents and the responses of calcification to global change, we postulate about the impacts that modulation may have on biomineralization. It is worth addressing the fact that surficial calcification (i.e., inorganic carbon content) and whole-thallus net calcification (i.e., buoyant weight) responses to OA and warming differed from each other and across CCA. The absence of a correlation between the two metrics can be explained by the respective portion of the thallus they represent. Surficial C_{inorg} content was quantified in the uppermost cell layers, whereas net calcification rates can reflect the change in $CaCO_3$ mass of the whole thallus (Langdon et al. 2010). It is important to note that growth (vertical and lateral), cell size, $CaCO_3$ density, and thallus thickness can vary within and across CCA taxa (Kamenos and Law 2010, Ragazzola et al. 2012, McCoy and
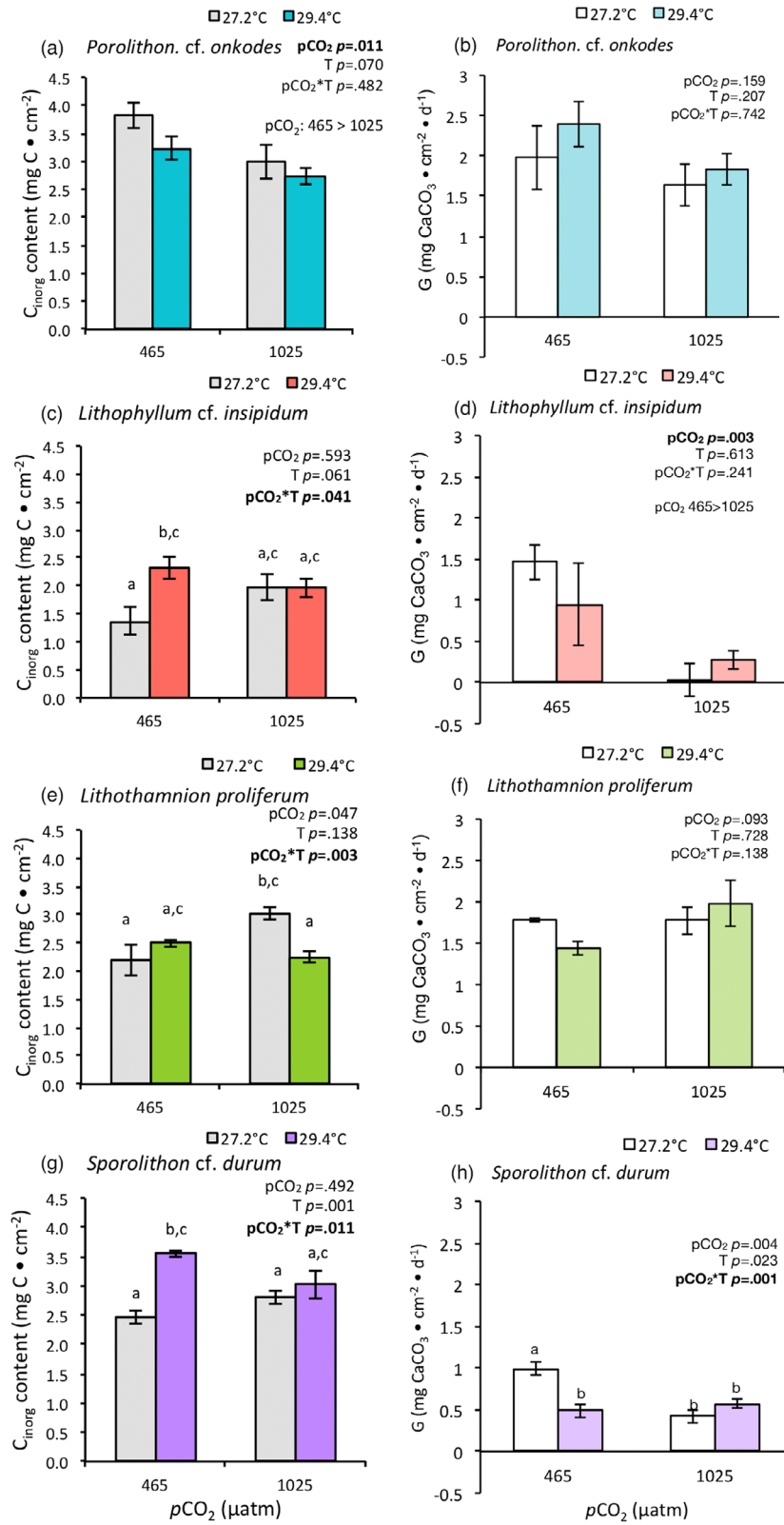
FIG. 6. Surficial calcification (C_{inorg} content) and whole-thallus net calcification (G) responses of *Porolithon* cf. *onkodes* (a, b), *Lithophyllum* cf. *insipidum* (c, d), *Lithothamnion proliferum* (e, f), and *Sporolithon* cf. *durum* (g, h) to the full factorial combination of ambient (465 µatm) and elevated (1025 µatm) pCO_2 levels and ambient (~27.2°C) and high (29.4°C) temperature levels. Values are means ± SE of $n = 4$–5. Significant differences ($P < 0.050$) between treatments resulting from Tukey HSD post hoc pairwise comparisons are indicated by unalike lowercase letters. [Color figure can be viewed at wileyonlinelibrary.com]

Ragazzola 2014). Calcite density can decrease at elevated temperature (Kamenos and Law 2010) and thallus thickness can be altered under OA (McCoy 2013, McCoy and Ragazzola 2014), which can have varied implications for growth and biomineralization. This means that the impacts of growth particularities cannot be teased out of our monosaccharide and surficial calcification data. While we acknowledge that this is a caveat, our findings still reveal important, novel associations between the general state of monosaccharide composition and surficial calcification across global change scenarios. Here we choose to focus on surficial calcification, as we believe it is more representative of the relationship in discussion.

The only common trend across all CCA species examined was increased Glc abundance under elevated pCO_2 or temperature, but this shift could affect species differently based on other constituents. This suggests that cellulose chains may increase in number and/or length across species, which in theory, if present as CMFs would provide increased surface area for potential crystallization. However, the lack of a concomitant increase in both GulA and ManA in *Porolithon* cf. *onkodes*, monomers of the potentially inducing polysaccharide alginate, could counteract the potential benefits of increased Glc in the cell wall. Indeed, a decrease in surficial calcification under elevated pCO_2 appears to corroborate this suggestion. Shifts in other constituents of *P.* cf. *onkodes* may also contribute; such as the simultaneous 231% increase in UNI-B. Interestingly, *Lithophyllum* cf. *insipidum* experienced increased surficial calcification while increasing Glc under elevated temperature, and this species increased UNI-B by only 30%. Research suggests some cell wall polymers actually inhibit high-Mg calcite biomineralization (Borowitzka and Larkum 1987), although the exact mechanisms are unclear (Wada et al. 1993, Long et al. 2014). It would be valuable to test whether there might be a threshold for modulation of sugars like UNI-B until it becomes inhibitory, and whether pCO_2 and/or temperature can interact with this effect differently across species. Although it is well known that net calcification rates can be directly suppressed by lowered pH, our novel findings of monosaccharide modulation under global change suggest an increased importance of considering the interplay of the organic matrix in biomineralization.

Predictions of shifts in discrete cell wall polysaccharides under global change could have implications for the structural nature and inducing capacity of the organic matrix. Xylans can form dimer, helical, or triple helical structures that can be physically significantly different from cellulose and mannans (Kloareg and Quatrano 1988, Stiger-Pouvreau et al. 2016). Xylans also commonly replace cellulose as structural polysaccharides in rhodophytes (Usov 2011). Thus, the suggested shifts in the cell wall matrix structure could have particularly serious implications for the function of *P.* cf. *onkodes*, as species of *Porolithon* are the most important reef-building algae in tropical reefs worldwide (Adey 1978, Littler and Littler 1984, Gabrielson et al. 2018). Structural compromise to reef framework stability will ultimately be dependent on biomineralization responses of CCA under OA and warming.

Moreover, temperature alone may have the potential to uniquely affect the organic matrix-biomineralization dynamic in particular reef-builders. Under the sole elevation of temperature, the capacity of *Lithothamnion proliferum* to increase surficial calcification coincides with a decrease in GulA content and methylated Gal substitution, which could have effects on the gelling and/or inducing capacity of its organic matrix. In *Sporolithon* cf. *durum*, there was an association between the capability of modulating monosaccharide abundances and ratios and increasing surficial calcification under the sole elevation of temperature, even though interactions with pCO_2 ultimately ameliorated these effects. Since this involved both the increase and decrease of five monosaccharides, the relative contribution of each constituent is somewhat ambiguous, but provides important grounds for further exploration. In *Porolithon* cf. *onkodes*, the decreased abundance of Man under elevated temperature, regardless of pCO_2, may indicate a modulation of mannan content, and thus matrix structure. Altogether, these findings reveal that organic matrix modulation is differentially impacted by temperature across CCA taxa.

Concluding remarks and future directions. Overall, by exploring the relationship between organic matrix constituents and biomineralization across CCA taxa and environmental change, this study shows that CCA species differ greatly in their organic matrix composition and have variable capacities for modulating monosaccharide abundance under OA and warming. This ability would result in different structural and inducing properties of organic matrices across species and environmental scenarios, which could impact biomineralization. Thus, the species-specific calcification responses to global warming and ocean acidification recorded to date (Martin and Gattuso 2009, Johnson and Carpenter 2012, Hofmann and Bischof 2014, McCoy and Ragazzola 2014, Cornwall et al. 2018) could suggest that the diversity of organic matrix composition across CCA taxa may be influencing the varied experimental responses. In order to further explore the relationship between discrete carbohydrate constituents, their regulation, and their relationship with calcification throughout the thallus, comparative studies should be carried out on the surficial thallus, perithallus, and hypothallus. Microscale analytical techniques can be used to overcome the challenge of biomass restrictions in CCA. For example,

Raman spectroscopy and synchrotron-based Fourier-transform infrared spectromicroscopy can be used to further characterize cell wall organic content and compare with mineralogy, Mg/Ca ratios, and calcifying fluid saturation state (DeCarlo et al. 2018, 2019, Valdespino-Castillo et al. 2021). In addition, it will be key to pair this information with genomic and proteomic data regarding the expression of (i) polysaccharide syntheses responsible for producing cell wall matrix constituents (e.g., cellulose, xylan, and mannan synthase proteins; Pauly et al. 2013, Zhu et al. 2019), and (ii) enzymes responsible for the addition and modification of side chain units (e.g., fucosyltransferase, galactosyltransferase, guluronosyltransferase; Pauly et al. 2013). Global change processes affect coralline algal calcification via a variety of mechanisms (e.g., direct effects on crystal biology, changes to algal metabolic processes, alterations to carbonate chemistry in the water column and calcifying fluid). However, our study provides new evidence suggesting that in addition to these previously identified mechanisms, the organic compounds in the cell wall matrix proposed to enable calcification also change under elevated OA and temperature and may thus serve as another crucial mechanism involved in global change response. Finally, our study shows the complexity of considerations needed to tease apart the processes contributing to how CCA respond under global change, all of which may have profound ramifications for the ability of reef-building coralline algae to continue to cement reef frameworks in a rapidly changing environment.

Adey, W. H. 1978. Algal ridges of the Caribbean sea and West Indies. *Phycologia* 17:361–7.

Adey, W. H. 1998. Coral reefs: algal structured and mediated ecosystems in shallow, turbulent, alkaline waters. *J. Phycol.* 34:393–406.

Adey, W. H., Townsend, R. & Boykins, W. 1982. The crustose coralline algae Rhodophyta (Corallinaceae) of the Hawaiian Islands. *Smithsonian Contrib. Mar. Sci.* 15:1–74.

Aguirre, J., Riding, R. & Braga, J. C. 2000. Diversity of coralline red algae: origination and extinction patterns from the Early Cretaceous to the Pleistocene. *Paleobiology* 26:651–67.

Al Abdallah, Q., Nixon, B. T. & Fortwendel, J. R. 2016. The enzymatic conversion of major algal and cyanobacterial carbohydrates to bioethanol. *Front. Energy Res* 4:36.

Bergstrom, E., Ordoñez, A., Ho, M., Hurd, C., Fry, B. & Diaz-Pulido, G. 2020. Inorganic carbon uptake strategies in coralline algae: Plasticity across evolutionary lineages under ocean acidification and warming. *Mar. Environ. Res.* 161:105107.

Bilan, M. I. & Usov, A. I. 2001. Polysaccharides of calcareous algae and their effect on the calcification process. *Russ. J. Bioorganic Chem.* 27:2–16.

Borowitzka, M. A. & Larkum, A. W. D. 1987. Calcification in algae: mechanisms and the role of metabolism. *Crit. Rev. Plant Sci.* 6:1–45.

Brownlee, C. & Taylor, A. 2004. Calcification in coccolithophores: a cellular perspective. *In* Thierstein, H. R. & Young, J. R. [Eds.] *Coccolithophores.* Springer, Berlin, Heidelberg, pp. 31–49.

Cases, M. R., Stortz, C. A. & Cerezo, A. S. 1994. Structure of the 'corallinans'—sulfated xylogalactans from *Corallina officinalis*. *Int. J. Biol. Macromol.* 16:93–7.

Comeau, S., Cornwall, C. E., DeCarlo, T. M., Krieger, E. & McCulloch, M. T. 2018. Similar controls on calcification under ocean acidification across unrelated coral reef taxa. *Glob. Chang. Biol.* 24:4857–68.

Cornwall, C. E., Comeau, S. & McCulloch, M. T. 2017. Coralline algae elevate pH at the site of calcification under ocean acidification. *Glob. Chang. Biol.* 23:4245–56.

Cornwall, C. E., Comeau, S., DeCarlo, T. M., Moore, B., D'Alexis, Q. & McCulloch, M. T. 2018. Resistance of corals and coralline algae to ocean acidification: physiological control of calcification under natural pH variability. *P. Roy. Soc. B Biol. Sci.* 285:20181168.

Cornwall, C. E., Diaz-Pulido, G. & Comeau, S. 2019. Impacts of ocean warming on coralline algal calcification: Meta-analysis, knowledge gaps, and key recommendations for future research. *Front. Mar. Sci* 6:186.

Daume, S., Brand-Gardner, S. & Woelkerling, W. J. 1999. Settlement of abalone larvae (*Haliotis laevigata* Donovan) in response to non-geniculate coralline red algae (Corallinales, Rhodophyta). *J. Exp. Mar. Biol. Ecol.* 234:125–43.

Dean, W. E. 1974. Determination of carbonate and organic matter in calcareous sediments and sedimentary rocks by loss on ignition; comparison with other methods. *J. Sediment. Res.* 44:242–8.

Dean, A. J., Steneck, R. S., Tager, D. & Pandolfi, J. M. 2015. Distribution, abundance and diversity of crustose coralline algae on the Great Barrier Reef. *Coral Reefs* 34:581–94.

DeCarlo, T. M., Ren, H. & Farfan, G. 2018. The origin and role of organic matrix in coral calcification: Insights from comparing coral skeleton and abiogenic aragonite. *Front. Mar. Sci* 5:170.

DeCarlo, T. M., Comeau, S., Cornwall, C. E., Gajdzik, L., Guagliardo, P., Sadekov, A., Thillainath, E. C., Trotter, J. & McCulloch, M. T. 2019. Investigating marine bio-calcification mechanisms in a changing ocean with in vivo and high-resolution ex vivo Raman spectroscopy. *Glob. Chang. Biol.* 25:1877–88.

Diaz-Pulido, G., Anthony, K. R. N., Kline, D. I., Dove, S. & Hoegh-Guldberg, O. 2012. Interactions between ocean acidification and warming on the mortality and dissolution of coralline algae. *J. Phycol.* 48:32–9.

Ferreira, L. G., Noseda, M. D., Gonçalves, A. G., Ducatti, D. R. B., Fujii, M. T. & Duarte, M. E. R. 2012. Chemical structure of the complex pyruvylated and sulfated agaran from the red seaweed *Palisada flagellifera* (Ceramiales, Rhodophyta). *Carbohydr. Res.* 347:83–94.

Frei, E. & Preston, R. D. 1961. Variants in the structural polysaccharides of algal cell walls. *Nature* 192:939–43.

Gabrielson, P. W., Hughey, J. R. & Diaz-Pulido, G. 2018. Genomics reveals abundant speciation in the coral reef building alga *Porolithon onkodes* (Corallinales, Rhodophyta). *J. Phycol.* 54:429–34.

Gee, J. M. & Knight-Jones, E. W. 1962. The morphology and larval behaviour of a new species of *Spirorbis* (Serpulidae). *J. Mar. Biolog. Assoc. UK* 42:641–54.

Gordon, G. D., Masaki, T. & Akioka, H. 1976. Floristic and distributional account of the common crustose coralline algae on Guam. *Micronesica* 12:247–77.

Goreau, T. F. 1961. On the relation of calcification to primary productivity in reef building organisms. *In* Lenhoff, H. H. & Loomis, W. F. [Eds.] *The Biology of Hydra and some other Coelenterates.* University of Miami Press, Miami, pp. 269–85.

Harrington, L., Fabricius, K., De'ath, G. & Negri, A. 2004. Recognition and selection of settlement substrata determine postsettlement survival in corals. *Ecology* 85:3428–37.

Hofmann, L. C. & Bischof, K. 2014. Ocean acidification effects on calcifying macroalgae. *Aquat. Biol.* 22:261–79.

Janot, K. G., Unda, F., Mansfield, S. D. & Martone, P. T. 2022. Evolutionary patterns in chemical composition and biomechanics of articulated coralline algae. *Integr. Comp. Biol.* 62:652–67.

Jeong, S. Y., Nelson, W. A., Sutherland, J. E., Peña, V., Le Gall, L., Diaz-Pulido, G., Won, B. Y. & Cho, T. O. 2021. Corallinapetrales and Corallinapetraceae: a new order and family of coralline red algae including *Corallinapetra gabrielii* comb. nov. *J. Phycol.* 57:849–62.

Johnson, M. D. & Carpenter, R. C. 2012. Ocean acidification and warming decrease calcification in the crustose coralline alga *Hydrolithon onkodes* and increase susceptibility to grazing. *J. Exp. Mar. Biol. Ecol.* 434:94–101.

Jorissen, H., Galand, P. E., Bonnard, I., Meiling, S., Raviglione, D., Meistertzheim, A. L., Hédouin, L., Banaigs, B., Payri, C. E. & Nugues, M. M. 2021. Coral larval settlement preferences linked to crustose coralline algae with distinct chemical and microbial signatures. *Sci. Rep.* 11:14610.

Kamenos, N. A. & Law, A. 2010. Temperature controls on coralline algal skeletal growth. *J. Phycol.* 46:331–5.

Kato, A., Baba, M. & Suda, S. 2011. Revision of the Mastophoroideae (Corallinales, Rhodophyta) and polyphyly in nongeniculate species widely distributed on Pacific coral reefs. *J. Phycol.* 47:662–72.

Kloareg, B. & Quatrano, R. 1988. Structure of the cell walls of marine algae and ecophysiological functions of the matrix polysaccharides. *Oceanogr. Mar. Biol. Ann. Rev.* 26:259–315.

Langdon, C., Gattuso, J. P. & Andersson, A. 2010. Measurements of Calcification and Dissolution of Benthic Organisms and 13 Communities. *In* Riebesell, U., Fabry, V. J., Hansson, L. & Gattuso, J. [Eds.] *Guide to Best Practices for Ocean Acidification Research and Data Reporting.* Publications Office of the European Union, Luxembourg, pp. 213–32.

Lee, R. E. 2018. *Phycology*, 5th edition. Cambridge University Press, Cambridge, 535 pp.

Little, A., Lahnstein, J., Jeffery, D. W., Khor, S. F., Schwerdt, J. G., Shirley, N. J., Hooi, M., Xing, X., Burton, R. A. & Bulone, V. 2019. A novel (1,4)-β-linked glucoxylan Is synthesized by members of the cellulose synthase-like F gene family in land plants. *ACS Cent. Sci.* 5:73–84.

Littler, M. M. & Littler, D. S. 1984. Models of tropical reef biogenesis: the contribution of algae. *In* Round, F. E. & Chapman, D. J. [Eds.] *Progress in Phycological Research*, Vol. 3. Biopress Ltd., Bristol, pp. 323–64.

Long, X., Ma, Y. & Qi, L. 2014. Biogenic and synthetic high magnesium calcite – a review. *J. Struct. Biol.* 185:1–14.

Lowenstam, H. A. 1981. Minerals formed by organisms. *Science* 211:1126–31.

Marsh, J. A., Jr. 1970. Primary productivity of reef-building calcareous red algae. *Ecology* 51:255–63.

Martin, S. & Gattuso, J. P. 2009. Response of Mediterranean coralline algae to ocean acidification and elevated temperature. *Glob. Chang. Biol.* 15:2089–100.

Martone, P. T., Estevez, J. M., Lu, F., Ruel, K., Denny, M. W., Somerville, C. & Ralph, J. 2009. Discovery of lignin in seaweed reveals convergent evolution of cell-wall architecture. *Curr. Biol.* 19:169–75.

Martone, P. T., Navarro, D. A., Stortz, C. A. & Estevez, J. M. 2010. Differences in polysaccharide structure between calcified and uncalcified segments in the coralline *Calliarthron cheilosporioides* (Corallinales, Rhodophyta). *J. Phycol.* 46:507–15.

Martone, P. T., Janot, K., Fujita, M., Wasteneys, G., Ruel, K., Joseleau, J. P. & Estevez, J. M. 2019. Cellulose-rich secondary walls in wave-swept red macroalgae fortify flexible tissues. *Planta* 250:1867–79.

McCoy, S. J. 2013. Morphology of the crustose coralline alga *Pseudolithophyllum muricatum* (Corallinales, Rhodophyta) responds to 30 years of ocean acidification in the Northeast Pacific. *J. Phycol.* 49:830–7.

McCoy, S. J. & Ragazzola, F. 2014. Skeletal trade-offs in coralline algae in response to ocean acidification. *Nature Clim. Change* 4:719–23.

McNicholl, C., Koch, M. S. & Hofmann, L. C. 2019. Photosynthesis and light-dependent proton pumps increase boundary layer pH in tropical macroalgae: a proposed mechanism to sustain calcification under ocean acidification. *J. Exp. Mar. Biol. Ecol.* 521:151208.

Nash, M. C., Uthicke, S., Negri, A. P. & Cantin, N. E. 2015. Ocean acidification does not affect magnesium composition or dolomite formation in living crustose coralline algae, *Porolithon onkodes* in an experimental system. *Biogeosciences* 12:5247–60.

Nash, M. C., Diaz-Pulido, G., Harvey, A. S. & Adey, W. 2019. Coralline algal calcification: a morphological and process-based understanding. *PLoS ONE* 14:e0221396.

Navarro, D. A. & Stortz, C. A. 2008. The system of xylogalactans from the red seaweed *Jania rubens* (Corallinales, Rhodophyta). *Carbohydr. Res.* 343:2613–22.

Navarro, D. A., Ricci, A. M., Rodríguez, M. C. & Stortz, C. A. 2011. Xylogalactans from *Lithothamnion heterocladum*, a crustose member of the Corallinales (Rhodophyta). *Carbohydr. Polym.* 84:944–51.

Okazaki, M., Furuya, K., Tsukayama, K. & Nisizawa, K. 1982. Isolation and identification of alginic acid from a calcareous red alga *Serraticardia maxima. Bot. Mar.* 25:123–31.

Oksanen, J., Blanchet, G., Friendly, M., Kindt, R., Legendre, P., McGlinn, D., Minchin, P. R., O'Hara, R. B., Simpson, G. L., Solymos, P., Stevens, M. H. H., Szoecs, E. & Wagner, H. 2019. vegan: Community Ecology Package, R package version 2.5-6.

Ozaki, H., Maeda, M. & Nisizawa, K. 1967. Floridean starch of a calcareous red alga, *Joculator maximus. J. Biochem.* 61:497–503.

Pauly, M., Gille, S., Liu, L., Mansoori, N., de Souza, A., Schultink, A. & Xiong, G. 2013. Hemicellulose biosynthesis. *Planta* 238:627–42.

Pavez, J., Silva, J. F. & Melo, F. 2005. Effects of alginic acid from marine algae on calcium carbonate electrodeposited coating. *J. Cryst. Growth* 282:438–47.

Peña, V., Vieira, C., Braga, J. C., Aguirre, J., Rösler, A., Baele, G., De Clerck, O. & Le Gall, L. 2020. Radiation of the coralline red algae (Corallinophycidae, Rhodophyta) crown group as inferred from a multilocus time-calibrated phylogeny. *Mol. Phylogenet. Evol.* 150:106845.

Pueschel, C. M. 1990. Cell structure. *In* Cole, K. M. & Seath, R. G. [Eds.] *Biology of the Red Algae.* Cambridge University Press, Cambridge, pp. 7–41.

Ragazzola, F., Foster, L. C., Form, A., Anderson, P. S. L., Hansteen, T. H. & Fietzke, J. 2012. Ocean acidification weakens the structural integrity of coralline algae. *Glob. Chang. Biol.* 18:2804–12.

Rahman, M. A. & Halfar, J. 2014. First evidence of chitin in calcified coralline algae: new insights into the calcification process of *Clathromorphum compactum. Sci. Rep.* 4:1–11.

Rahman, M. A., Halfar, J., Adey, W. H., Nash, M., Paulo, C. & Dittrich, M. 2019. The role of chitin-rich skeletal organic matrix on the crystallization of calcium carbonate in the crustose coralline alga *Leptophytum foecundum*. *Sci. Rep.* 9:11869.

Rees, D. A. & Welsh, E. J. 1977. Secondary and tertiary structure of polysaccharides in solutions and gels. *Angew. Chem. Int. Ed. Engl.* 16:214–24.

Ringeltaube, P. & Harvey, A. 2000. Non-geniculate coralline algae (Corallinales, Rhodophyta) on Heron Reef, Great Barrier Reef (Australia). *Bot. Mar.* 43:431–54.

Rodríguez-Gacio, M. d. C., Iglesias-Fernández, R., Carbonero, P. & Matilla, Á. J. 2012. Softening-up mannan-rich cell walls. *J. Exp. Bot.* 63:3976–88.

Rowley, R. J. 1989. Settlement and recruitment of sea urchins (*Strongylocentrotus* spp.) in a sea-urchin barren ground and a kelp bed: are populations regulated by settlement or post-settlement processes? *Mar. Biol.* 100:485–94.

Siegel, B. Z. & Siegel, S. M. 1973. The chemical composition of algal cell walls. *Crit. Rev. Microbiol.* 3:1–26.

Steneck, R. S. 1986. The ecology of coralline algal crusts: convergent patterns and adaptive strategies. *Annu. Rev. Ecol. Syst.* 17:273–303.

Stiger-Pouvreau, V., Bourgougnon, N. & Deslandes, E. 2016. Carbohydrates from seaweeds. *In* Fleurence, J. & Levine, I. [Eds.] *Seaweed in Health and Disease Prevention.* Academic Press, San Diego, pp. 223–74.

Stortz, C. A. & Cerezo, A. S. 2000. Novel findings in carrageenans, agaroids and "hybrid" red seaweed galactans. *Curr. Top. Phytochem.* 4:121–34.

Takano, R., Hayashi, J., Hayashi, K., Hara, S. & Hirase, S. 1996. Structure of a water-soluble polysaccharide sulfate from the red seaweed *Joculator maximus* Manza. *Bot. Mar.* 39:95–102.

Tarte, D. & Hughes, T. 2020. Review of State Party Report on the state of conservation of the Great Barrier Reef World Heritage Area (Australia). Report prepared for the Australian Marine Conservation Society, pp. 1–9.

Tsekos, I. 1999. The sites of cellulose synthesis in algae: diversity and evolution of cellulose-synthesizing enzyme complexes. *J. Phycol.* 35:635–55.

Turvey, J. R. & Simpson, P. R. 1966. Polysaccharides from *Corallina officinalis*. *In* Young, E. G. & McLachlan, J. L. [Eds.] *Proceedings of the Fifth International Seaweed Symposium.* Halifax. Pergamon Press, London, pp. 323–7.

Usov, A. I. 1992. Sulfated polysaccharides of the red seaweeds. *Food Hydrocoll.* 6:9–23.

Usov, A. I. 2011. Polysaccharides of the red algae. *In* Horton, D. [Ed.] *Advances in Carbohydrate Chemistry and Biochemistry.* Academic Press, Oxford, pp. 115–217.

Usov, A. I. & Zelinsky, N. D. 2013. Chemical structures of algal polysaccharides. *In* Domínguez, H. [Ed.] *Functional Ingredients from Algae for Foods and Nutraceuticals.* Woodhead Publishing, Cambridge, pp. 23–86.

Usov, A. I., Bilan, M. I. & Klochkova, N. G. 1995. Polysaccharides of Algae. 48. Polysaccharide Composition of Several Calcareous Red Algae: Isolation of Alginate from *Corallina pilulifera* P. et R. (Rhodophyta, Corallinaceae). *Bot. Mar.* 38:43–51.

Valdespino-Castillo, P. M., Bautista-García, A., Favoretto, F., Merino-Ibarra, M., Alcántara-Hernández, R. J., Pi-Puig, T., Castillo, F. S., Espinosa-Matías, S., Holman, H. Y. & Blanco-Jarvio, A. 2021. Interplay of microbial communities with mineral environments in coralline algae. *Sci. Total Environ.* 757:143877.

Venkatesan, J., Bhatnagar, I., Manivasagan, P., Kang, K. H. & Kim, S. K. 2015. Alginate composites for bone tissue engineering: a review. *Int. J. Biol. Macromol.* 72:269–81.

Viola, R., Nyvall, P. & Pedersén, M. 2001. The unique features of starch metabolism in red algae. *Proc. R. Soc. Lond. B Biol. Sci.* 268:1417–22.

Vreeland, V. & Kloareg, B. 2000. Cell wall biology in red algae: divide and conquer. *J. Phycol.* 36:793–7.

Wada, N., Okazaki, M. & Tachikawa, S. 1993. Effects of calcium-binding polysaccharides from calcareous algae on calcium

carbonate polymorphs under conditions of double diffusion. *J. Cryst. Growth* 132:115–21.

Zhu, X., Xin, X. & Gu, Y. 2019. Cellulose and hemicellulose synthesis and their regulation in plant cells. *In* Cohen, E. & Merzendorfer, H. [Eds.] *Extracellular Sugar-Based Biopolymers Matrices.* Springer International Publishing, Cham, pp. 303–53.

Supporting Information

Additional Supporting Information may be found in the online version of this article at the publisher's web site:

Appendix S1. Supplementary Methods.

Figure S1. Linear regressions comparing the relationships between surficial calcification (C_{inorg} content) and whole-thallus net calcification (G) across pCO_2 and temperature treatments in (A) *Porolithon* cf. *onkodes*, (B) *Lithothamnion proliferum*, (C) *L. proliferum*, and (D) *Sporolithon* cf. *durum*. Values are means of $n = 3$–5.

Table S1. Mean relative abundance of monosaccharides $\pm$ SE ($n = 4$–5) under the full factorial combination of ambient (465 μatm) and elevated (1160 μatm) pCO_2 and ambient (27.2°C) and elevated (29.4°C) temperature in *Porolithon* cf. *onkodes*, *Lithothamnion proliferum*, *Lithophyllum* cf. *insipidum*, and *Sporolithon* cf. *durum*. Tukey HSD post hoc pairwise comparisons from two-way ANOVAs are indicated in superscript where present. Where there was a main pCO_2 effect, asterisks indicate the pCO_2 level with significantly greater values. Where there was a main temperature effect, bolded data indicate the temperature level with significantly greater values. Where an interactive effect between pCO_2 and temperature was present, unalike lowercase letters indicate significant differences between treatments.

Table S2. Two-way ANOVA results showing the effects of pCO_2 (two levels) and temperature (two levels) on Total Monosaccharide Concentration (μM; excluding Glucose) for *Porolithon* cf. *onkodes*, *Lithophyllum* cf. *insipidum*, *Lithothamnion proliferum*, and *Sporolithon* cf. *durum*.

Table S3. Two-way ANOVA results showing the effects of pCO_2 (two levels) and temperature (two levels) on monosaccharide abundances for *Porolithon* cf. *onkodes*, *Lithophyllum* cf. *insipidum*, *Lithothamnion proliferum*, and *Sporolithon* cf. *durum*.

Table S4. Two-way ANOVA results showing the effects of pCO_2 (two levels) and temperature (two levels) on net calcification (G) and surficial C_{inorg} content for *Porolithon* cf. *onkodes*, *Lithophyllum* cf. *insipidum*, *Lithothamnion proliferum*, and *Sporolithon* cf. *durum*. G data for *P.* cf. *onkodes* was log-transformed.